

Acoustical analysis and model-based sound synthesis of the kantele^{a)}

Cumhur Erkut^{b)} and Matti Karjalainen

Laboratory of Acoustics and Audio Signal Processing, Helsinki University of Technology, Espoo, Finland

Patty Huang

Center for Computer Research in Music and Acoustics, Stanford University, Stanford, California 94305-8180

Vesa Välimäki^{c)}

Laboratory of Acoustics and Audio Signal Processing, Helsinki University of Technology, Espoo, Finland

(Received 3 January 2002; revised 3 July 2002; accepted 3 July 2002)

The five-string Finnish kantele is a traditional folk music instrument that has unique structural features, resulting in a sound of bright and reverberant timbre. This article presents an analysis of the sound generation principles in the kantele, based on measurements and analytical formulation. The most characteristic features of the unique timbre are caused by the bridgeless string termination around a tuning pin at one end and the knotted termination around a supporting bar at the other end. These result in prominent second-order nonlinearity and strong beating of harmonics, respectively. A computational model of the instrument is also formulated and the algorithm is made efficient for real-time synthesis to simulate these features of the instrument timbre. © 2002 Acoustical Society of America. [DOI: 10.1121/1.1504858]

PACS numbers: 43.75.Gh, 43.75.Wx [NHF]

I. INTRODUCTION

The *kantele*¹ refers to a group of plucked string instruments that have been common in traditional folk music in Finland, its neighboring region in Northwest Russia, and the Baltic states.^{2,3} The instrument and its variations are called the *kannel* in Estonia, the *kanklės* in Lithuania, the *kokle* in Latvia, and the *gusli* in Russia.² They belong to the family of zithers. The five-string Finnish kantele has a significant role in Finnish folklore as the instrument of rune singers, and in Finnish mythology, especially in the Kalevala, the collection of ancient Finnish runes.⁴ It is estimated that the origins of the kantele are more than 1000 years old.

The traditional Finnish kantele has five strings and a body made of a single piece of wood. The traditional instrument illustrated in Fig. 1 is hollowed out at the top and the opening is covered by a top plate with a sound hole (X-shaped in this model). Strings are terminated at the wider end around wooden tuning pegs. At the other end the strings are attached with a knotted termination around the *varras*, a bar typically made of metal, in a U-shaped raised body structure (the *ponsi*).

At the end of 18th century the instrument started an evolution to new forms. The body of the kantele was even-

tually constructed of separate plates instead of a single piece of wood, and the wooden tuning pegs were replaced by metallic tuning pins. This type of the instrument is the focus of the present study. To be able to play more complex music the kantele was made larger and equipped with more strings—for example, 9 to 15 strings. For compatibility with concert music, a *concert kantele* has been developed since the 1920's to contain up to 45 strings, with a range of about five octaves. The challenge of playing in different keys and with chromatic notes was solved by including a lever mechanism, similar to that of a concert harp, for rapid change of tuning.

The kantele has a characteristic sound that is bright and reverberant.⁵ Only recently, acoustical studies have been carried out on the instrument to reveal the features that make the unique sound. In a previous work,⁶ based on measurements and signal analysis, specific properties of string terminations were reported as prominent sources of the characteristic kantele tone. A recent study focused on the body vibrations of a general class of the Baltic psalteries.⁷

The objective of the present article is to give a systematic and thorough presentation of the instrument, showing the

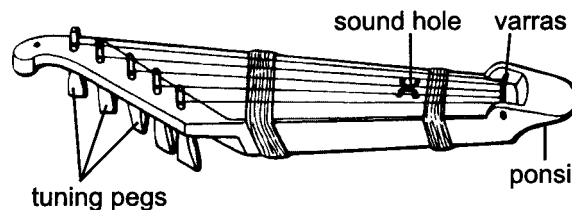


FIG. 1. A Finnish traditional five-string kantele made by hollowing out the top of a single wood block and covering it with a top plate. The strings are attached, without a bridge, to the tuning pegs at the left-hand side and to a bar at the right-hand side. After Sadie (Ref. 2).

^{a)}Portions of this work were presented in "Analysis, modeling, and real-time sound synthesis of kantele, a traditional Finnish string instrument," Proceedings of IEEE International Conference on Acoustics, Speech, and Signal Processing, Minneapolis, MN, April 1993, and "Nonlinear modeling and synthesis of the kantele—A traditional Finnish string instrument," Proceedings of International Computer Music Conference, Beijing, China, October 1999.

^{b)}Electronic mail: cumhur.erkut@hut.fi

^{c)}Part of the work done while at Tampere University of Technology, Pori School of Technology and Economics, Pori, Finland.

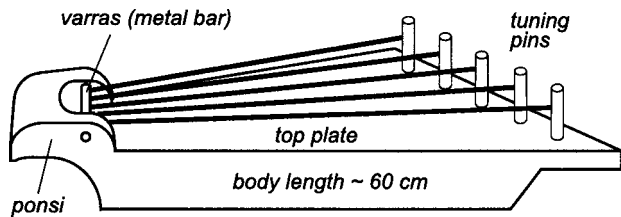


FIG. 2. Structure of a five-string kantele used in most experiments of this study. The body is made hollow from the bottom and left open. After Karjalainen *et al.* (Ref. 6).

behavior of kantele strings, body, and sound radiation. This article starts with a structural description of an open-body kantele, as well as playing techniques and tuning of the instrument in Sec. II. Section III presents an acoustical analysis of the instrument. The terminations of the strings deserve special attention since they introduce strong beating and nonlinear effects to the sound. The nonlinear vibrations of the kantele strings are of exceptional importance in producing the resulting timbre. The properties of body vibrations as a response to the driving forces on the strings are demonstrated. In Sec. IV, a computationally efficient sound synthesis algorithm is presented. The algorithm captures the most essential properties of the kantele sound, and allows for the synthesis of kantele tones in real time.

II. DESCRIPTION OF THE INSTRUMENT

A. Construction and tuning

Our study focuses on a present-day version of the traditional five-string kantele, illustrated in Fig. 2. The body is hollowed open at the bottom and thus there is no need for a sound hole. This model was used due to its structural simplicity.

The five metal strings are of equal diameter (0.35 mm) with lengths ranging from 32.5 to 47.8 cm. At the narrower end of the kantele the strings are wound once around the varras and knotted as shown in Fig. 3. At the opposite end the metal tuning pins are screwed directly into the soundboard that is the top plate of the body, and the strings are terminated directly around the pins without a bridge (Fig. 4). Such terminations are unique structural features of the instrument.

The five-string kantele is tuned to a diatonic scale, and the third string can be tuned to a major third, minor third, or somewhere in between. The tuning of the lowest string is

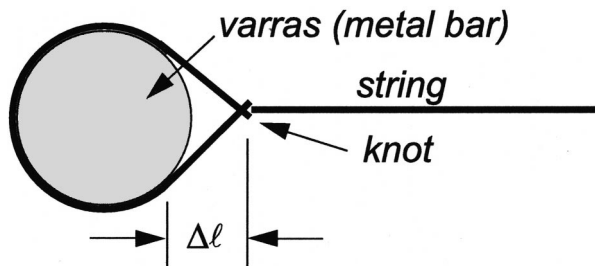


FIG. 3. String with a knot termination around the varras (metal bar). Effective string lengths differ by Δl for different vibration directions. After Karjalainen *et al.* (Ref. 6).

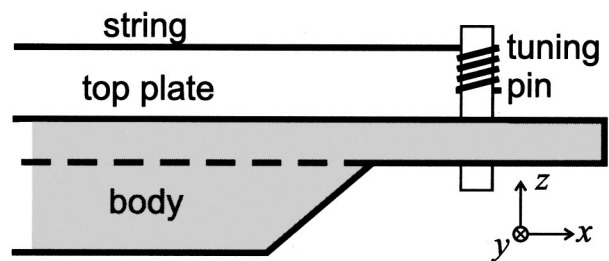


FIG. 4. String termination around a tuning pin without a bridge. A reference coordinate system is indicated at the bottom part of the figure. After Karjalainen *et al.* (Ref. 6).

typically near D_4 (294 Hz), although transposition of several semitones (up or down) is also common. In our experiments, the lowest string has been tuned to $E\flat_4$ (311 Hz).

B. Playing techniques

The five-string kantele is played across one's lap or on a table, with the shortest string closest to the player. There are regional and personal variations in playing technique, but the most common traditional way is to interleave fingers of left and right hands, with one finger for each string and the right thumb playing the highest string. A string is plucked upwards so that all other strings remain free to vibrate. This makes a reverberant sound. Damping of strings or plucking horizontally so that the finger damps the next string can be used in modern playing. Another technique that yields an even brighter sound is to strike a string by fingernail. These techniques can also be combined. Playing can consist of a melody line, accompaniment, or both, although in traditional playing there was often no clear distinction between them.

III. ACOUSTICAL ANALYSIS OF THE KANTELE

A. Observations of kantele tones

Figure 5 shows the amplitude envelope trajectories of the first three harmonics of (a) a softly plucked and (b) a strongly plucked kantele tone. The measurements were carried out in an anechoic chamber, where the microphone

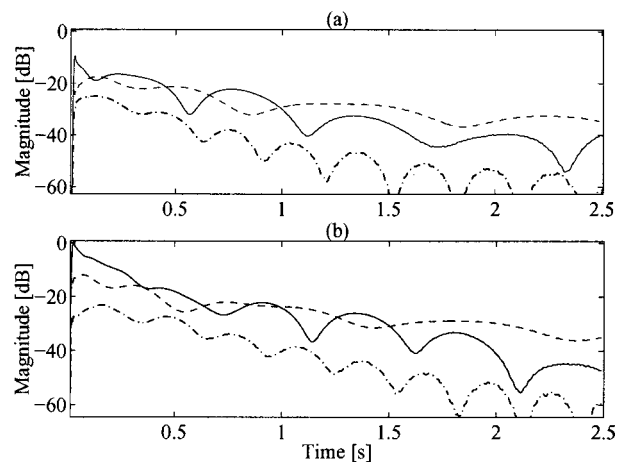


FIG. 5. Envelope trajectories of kantele tones. The first harmonic is shown with a dashed line, the second with a solid line, and the third with a dash-dotted line. (a) A softly plucked tone and (b) a strongly plucked tone. The plucking point is the midpoint of the third string.

(B&K 4145) was fixed at a distance of 1 meter above the top plate of the instrument. The plucking point is the midpoint of the third string so that, according to the linear theory of string vibration, even harmonics should be absent.⁸

The first noticeable feature of the kantele tones in Fig. 5 is a strong beating of harmonics. This phenomenon is explained in Sec. III B. Another feature is the presence and dominance of the second harmonic. The initial magnitude of the second harmonic is approximately 10 dB higher in the case of a strong pluck in Fig. 5(b), compared to that of the soft pluck in Fig. 5(a). The generation and the amplitude dependence of the second harmonic indicate a nonlinear mechanism, which is the subject of Sec. III C. Section III D presents the formulation of a nonlinear longitudinal force component, and Sec. III E derives an analysis method. In Sec. III F we demonstrate by measurements how the body of the instrument responds to the forces applied on a tuning pin. Within the same section, we also briefly discuss the properties of the body of the traditional kantele, as well as the energy transfer between the strings.

Throughout the discussion we use the following convention to refer to three orthogonal vibration directions. A rectangular reference coordinate system is shown in Fig. 4. The x axis is along the strings so that the varras is at $x=0$ and a tuning pin is at $x=L$. The y axis is parallel to the top plate, and the z axis is in the direction of the normal to the top plate. The *longitudinal*, *horizontal*, and *vertical* directions are aligned with the unit vectors of the x , y , and z axes, respectively. When we refer to a vibration in the plane spanned by horizontal and vertical unit vectors, we use the term *transverse*.

B. Analysis of the beating

The observed beating in Fig. 5 is essentially a result of the knotted termination at the varras. This termination dictates two different effective string lengths, one for the vertical and another for the horizontal vibration, with a length difference of Δl (see Fig. 3). For the vertical polarization, the knot is the termination point, whereas for the horizontal polarization, the contact point to the varras is the termination point.^{6,7} As a consequence, the vertical and horizontal fundamentals have a constant frequency difference Δf_0 that creates the beats.

To verify this explanation, we used a modified kantele,⁹ where the string is terminated without a knot, but otherwise the construction is identical to that of the regular kantele. Figure 6 shows the first three harmonic envelopes extracted from (a) regular and (b) knotless kantele tones of the same frequency ($f_0=415$ Hz). In the knotless design the beating vanishes, confirming our explanation.

The frequency difference of the two transverse polarizations is related to the length difference Δl by

$$\Delta f_0 = f_{0,z} - f_{0,y} = \frac{c}{2l} - \frac{c}{(2l + \Delta l)} = \frac{\Delta l}{l} f_{0,y}, \quad (1)$$

where l is the effective length of the string between the tuning pin and the knot (see Fig. 3), $c = \sqrt{T/\rho}$ is the transverse propagation speed determined in terms of the string tension T

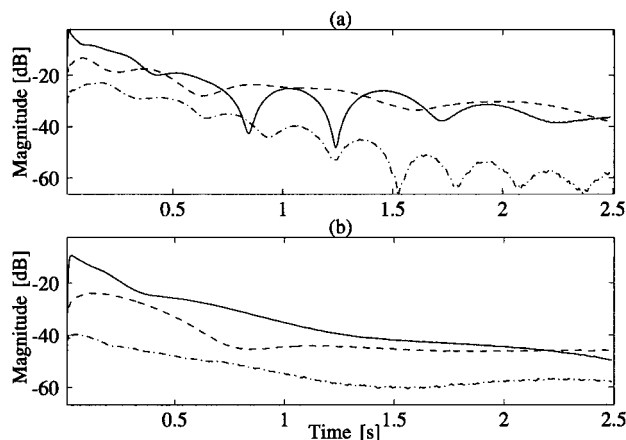


FIG. 6. Envelope trajectories of tones from a normal (a) and a modified (b) kantele. The first harmonic is shown with a dashed line, the second with a solid line, and the third with a dash-dotted line. The plucking strength is medium and the plucking point is the midpoint of the third string. The strong beating does not appear in the knotless kantele.

and the linear mass density ρ , and Δl is the difference of the effective string length for different polarizations. The frequency difference can also be confirmed experimentally by analyzing the amplitude envelope of the first harmonic of recorded kantele tones and by extracting the beating frequency by fitting a sine wave using the nonlinear least-squares method.¹⁰ To avoid confusion, we refer to the extracted fundamental frequency difference as $\Delta f_{0,ex}$.

Figure 7 presents an example where the linear trend and mean of the envelope of the first harmonic have been removed on a logarithmic (dB) scale in order to compensate the natural decay of the harmonic, and a sine wave has been fitted to the available data above the noise level. We observed experimentally that the plucking direction slightly alters the beating pattern. Note that, because of nonlinear coupling between different polarizations, the string exhibits an elliptical vibration pattern shortly after the initial pluck, regardless of the initial excitation direction.¹¹ Therefore, we use an average of two cases, a horizontal and a vertical pluck. We noticed that this method yields a good estimate of

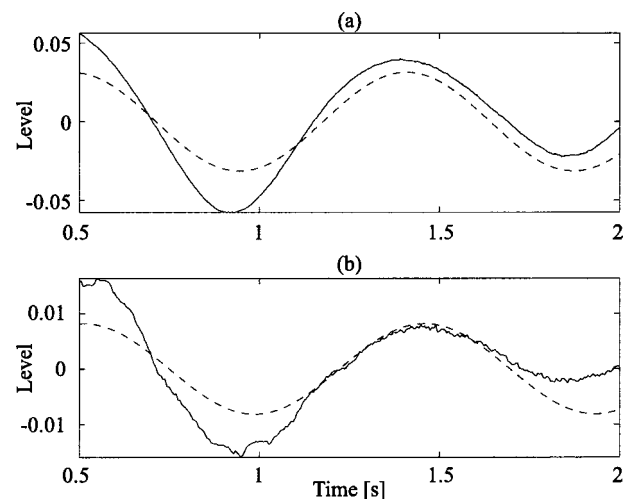


FIG. 7. Beating of the first harmonic (solid line) in a kantele tone plucked horizontally (a) and vertically (b), with a nonlinear least-squares sine wave fit (dashed line).

TABLE I. The fundamental frequencies $f_{0,y}$ of the horizontal polarizations, the frequency differences Δf_0 according to Eq. (1), and the extracted frequency differences $\Delta f_{0,ex}$ for the five strings of the kantele. All quantities are given in hertz.

String	#1	#2	#3	#4	#5
$f_{0,y}$	465.2	414.5	391.3	354.5	314.3
Δf_0	1.50	1.28	1.10	0.95	0.76
$\Delta f_{0,ex}$	1.30	1.04	1.07	0.97	0.77

the difference in the fundamental frequency of vibration of the two polarizations.

Table I shows the fundamental frequencies of horizontal polarizations for the five strings of the kantele and the frequency differences Δf_0 , obtained by inserting the measured length l and the effective length difference Δl for each string into Eq. (1). The extracted frequency differences $\Delta f_{0,ex}$ are obtained by the sine-fitting method described above. Δf_0 and $\Delta f_{0,ex}$ are in qualitative agreement. The differences are caused by the imaginary part of the input admittance at the tuning pin,¹² and by the nonlinearities discussed in the next section.

C. Tension modulation nonlinearity

Unlike an ideal flexible string, a real string, such as a kantele string, is linear to the first-order approximation only. Reformulation of the wave equation to include these second-order terms has a relatively long history (see Ref. 13 for a review). The major cause of nonlinearities is that any small transverse displacement of the string makes a second-order change in its length and therefore in its tension. By assuming fixed boundary conditions and using an excitation force of a frequency close to that of the first mode of the string, the tension modulation is shown both analytically and experimentally to cause a fundamental frequency descent,^{14,15} a whirling motion,^{16–18} coupling between different modes and directions,^{12,15,19} and amplitude jumps.^{11,20}

Legge and Fletcher showed that the generation of missing modes in a musical instrument is only possible when a realistic model of the termination at the bridge is taken into account.¹² However, they concluded that with a termination similar to that of a bridgeless kantele, the nonlinearities cannot provide subsequent excitation of any of the missing even harmonics, if the string is initially plucked near its center. Moreover, according to their theory, even in case of a termination by a guitar-like bridge, the unexcited modes should exhibit a slow build-up (typically around 100 ms). The behavior of the second harmonic in Figs. 5 and 6—specifically, the observed rapid onset with a high initial level—is not consistent with their conclusion.

This inconsistency is clarified by noting the structural differences between the kantele and other plucked-string instruments. In most string instruments, the bridge is the usual termination point of the strings at one end, and it is relatively rigid in the longitudinal direction.⁸ An important function of the bridge is to transmit the transverse forces of the string to the body of the instrument, and hence the longitudinal force component is usually filtered out. A plucked-string body is

typically not responsive to the longitudinal forces below 1 kHz.²¹

In the kantele, the tuning pins are not rigid in the longitudinal direction and transmit any longitudinal force efficiently to the body. As will be demonstrated in the following, nonlinear mechanisms caused by the tension modulation create a longitudinal force component, called the *tension modulation driving force*,²² or TMDF for short, which accounts for the instantaneous onset and high initial amplitude of the second harmonic in Figs. 5 and 6.

A similar mechanism has been observed in an acoustical guitar, an orchestral harp, and a piano.²³ The partials thus generated are termed as *phantom partials*, and it has been concluded that any plucked-string or struck-string instrument that is susceptible to longitudinal string forces could produce phantom partials. The phantom partials are observed between 1–3 kHz. Measurement results indicate that the kantele body is susceptible to the longitudinal TMDF. The TMDF has a significant effect on the lowest partials, thus on the timbre, as will be demonstrated in the following.

D. TMDF formulation

In order to obtain the TMDF exerted on a tuning pin, we ignore the effective length difference in transverse directions discussed in Sec. III B and rely on the knotless kantele analysis data. Moreover, the string is taken to be linearly elastic, the inharmonicity caused by string stiffness (dispersion) is assumed negligible, and the cross-sectional area of the string (and hence its density) is taken to be constant during the vibration.

For steel strings, the transverse propagation speed is usually smaller than 10% of the longitudinal propagation speed. This practically means that the first longitudinal component of the string vibration has a frequency higher than the tenth transverse harmonic. However, here we focus on the lowest harmonics of the kantele tones. This fact justifies why we assume that TMDF is the only longitudinal force component acting on a tuning pin and neglect the effects of longitudinal wave propagation. Note that the same argument has also been used in several analytical treatments of nonlinear string vibrations.^{12,16}

Under these assumptions, elongation of the string l_{dev} may be expressed as the deviation from the nominal string length L

$$l_{dev} = \int_0^L \left[1 + \left(\frac{\partial y}{\partial x} \right)^2 + \left(\frac{\partial z}{\partial x} \right)^2 \right]^{1/2} dx - L$$

$$\approx \int_0^L \frac{1}{2} \left[\left(\frac{\partial y}{\partial x} \right)^2 + \left(\frac{\partial z}{\partial x} \right)^2 \right] dx, \quad (2)$$

where x , y , and z denote the spatial variables (see Fig. 4) along the longitudinal, horizontal, and vertical directions, respectively, and the approximation is obtained by neglecting all but the first terms of Taylor series expansion of the slopes. If the supports are rigid, the tension yields

$$T = T_0 + ES \frac{l_{dev}}{L}, \quad (3)$$

where T_0 is the nominal tension of the string in rest, E is Young's elastic modulus of string material, and S is the cross-sectional area of the string. It is customary^{8,15} to define the longitudinal force exerted on the pin as

$$F_x(T) \approx -T|_{x=L} = -\left(T_0 + ES \frac{l_{\text{dev}}}{L}\right). \quad (4)$$

Equation (4) is the analytical expression of TMDF. The negative sign indicates that the force is pulling the tuning pin towards the center of the instrument. There is a similar TMDF component acting on the varras at $x=0$ with a positive sign.

The eigenfunctions for the lossy wave equation in the two transverse directions are exponentially decaying sinusoids with amplitudes $a_{y,m}$ and $a_{z,n}$, where m and n indicate the harmonic numbers for the horizontal direction y and vertical direction z , respectively. The Fourier coefficients $a_{y,m}$ and $a_{z,n}$ have the physical dimension of meters. Inserting the eigenfunctions in Eq. (4) and neglecting terms of fourth- and higher order in $a_{y,m}/L$ and $a_{z,n}/L$, TMDF can be approximated as

$$F_x(T) \approx -T_0 - \frac{\pi^2 ES}{8L^2} \times \left\{ \sum_m m^2 a_{y,m}^2 [1 - \cos(2\omega_{y,m}t + \phi_{y,m})] e^{-2t/\tau_{y,m}} + \sum_n n^2 a_{z,n}^2 [1 - \cos(2\omega_{z,n}t + \phi_{z,n})] e^{-2t/\tau_{z,n}} \right\}, \quad (5)$$

where ω , ϕ , and τ are the frequency, initial phase, and time constant of the decay, respectively, corresponding to a particular mode.

Equation (5) suggests that each transverse harmonic contributes to the TMDF with two exponentially decaying components within the square brackets. The first terms do not oscillate, and they are the primary cause of the fundamental frequency descent.^{14,15} As will be shown later, the fundamental frequency descent in kantele tones can be used to extract information for the nonlinear behavior.²⁴ The oscillatory terms have twice the frequency and one half the decay times of the corresponding harmonics.

Given an initial displacement consisting of odd harmonics only, according to Eq. (5), the TMDF components that have twice the fundamental frequency are generated solely by the first harmonic of each polarization. Figure 8 illustrates the TMDF acting on the tuning pin in the absence of the vertical component. The top part of the figure depicts the horizontal fundamental y_1 of unity amplitude ($a_{y,1}=1$) that decays with its characteristic rate. The resulting TMDF pulls the tuning pin towards the center of the instrument twice during one period of the fundamental, and decays twice as fast.

In particular, if the initial displacement consists only of a single-polarization fundamental (e.g., in the y direction), and if the constant tension T_0 is suppressed, the time-varying part of Eq. (5) becomes

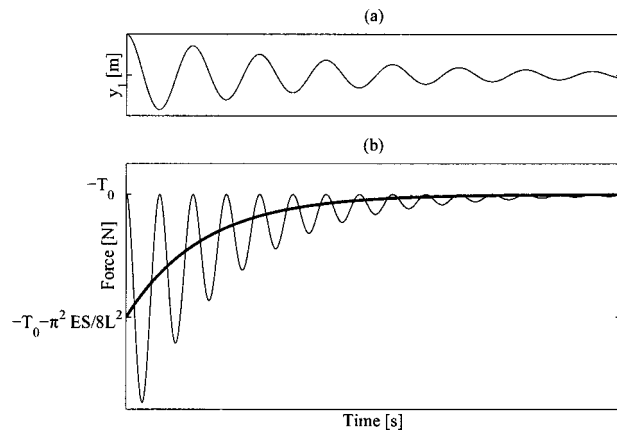


FIG. 8. The illustration of the TMDF for a single polarization case. (a) The exponentially decaying fundamental y_1 of unity amplitude. (b) The corresponding TMDF. The thick line is the component that causes the fundamental frequency descent, and the thin curve is the oscillatory component.

$$F_x(t) = -\frac{\pi^2 ES}{8L^2} (a_{y,1}^2 e^{-2t/\tau_{y,1}}) (1 - \cos(2\omega_{y,1}t + \phi_{y,1})). \quad (6)$$

Equation (6) is essentially the same in form with the dimensionless nonlinear mixing force given in Ref. 23 [see Eq. (3) in the reference]. It also suggests that $F_x(t)$ may be related to the dilated eigenfunction $y_1(x, 2t)$ by appropriate scaling and phase shifting. This property may be utilized as an analysis procedure. We present such an analysis procedure in the next subsection.

The kantele responds as a passive, linear system to the forces applied on its tuning pins. Therefore, some part of the TMDF is transmitted to the body, some part of it is reflected, and the rest is dissipated. We first concentrate on reflection.

The frequency difference of transverse and longitudinal modes, as stated in the previous section, indicates that the reflected TMDF component cannot be efficiently coupled to a longitudinal mode. It may, however, generate a transverse mode. The famous experiment of Melde demonstrates the possibility of the missing transverse mode generation by driving a string from one end in the longitudinal direction.²⁰ A recent study²⁵ shows that the three-dimensional admittance matrix of a musical instrument may interchange energy between longitudinal and transverse directions. This property is proved to be important in nonlinear generation of missing modes.¹²

If the TMDF is coupled back to the string by either mechanism, a generated transverse second harmonic should exhibit a build-up onset until the coupled energy is balanced by internal losses. After the balance instant, the second harmonic should decay with a characteristic rate that is independent of the first harmonic and governed only by the string and body properties. The tuning pin velocity measurements in transverse directions indicate the existence of such a component. However, the velocity magnitude of the generated transverse harmonic is typically 20 dB lower than the magnitude of the first harmonic. In terms of the forces, this difference is roughly 30 dB. We therefore conclude that the instantaneous onset and high initial amplitude of the second harmonic in Figs. 5 and 6 are caused by the TMDF compo-

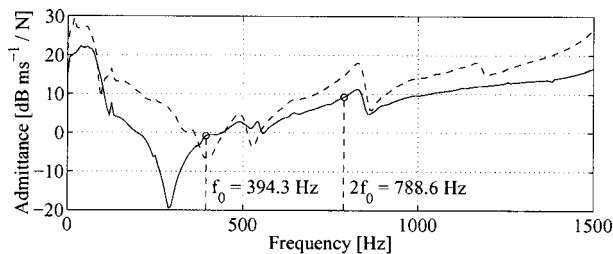


FIG. 9. The magnitude of the admittance measured in the longitudinal (solid) and horizontal (dashed) directions. The admittance values in the longitudinal direction corresponding to the first and second harmonics are indicated with small circles.

ment that is transmitted to the body and in turn radiated. Next, we discuss an analysis procedure to verify this explanation.

E. T MDF analysis

Consider Eq. (5) for $m=n=1$ and $a_{y,1}=a_{z,1}=a_1$. The equality of the initial amplitudes can be assured by deflecting the string along bisection of the transverse unit vectors (see Fig. 4). In this case, the oscillatory part of the T MDF yields

$$F_{osc} = 2(a_1)^2 \frac{\pi^2 ES}{8L^2} \xi(2t), \quad (7)$$

where $\xi(2t)$ is the normalized first harmonic that can be extracted from a velocity measurement using a bandpass filter, and then by dilating the filtered signal by a factor of 2. The dilation can simply be carried out by downsampling. The T MDF component thus calculated can be filtered with a premeasured input admittance function of the tuning pin and converted to the longitudinal velocity. The measured and calculated magnitude envelopes of the second harmonics are then compared. Similarly, the first harmonic can be extracted from a recorded tone, and the calculated T MDF component can be converted to the sound pressure by filtering it with the longitudinal body response.

The details of an experiment, in which the third string of the kantele was tuned to $f_0 = 394$ Hz, are described below. In the experiment, we used velocity data. The length of the string is 0.4015 m, and its diameter is 0.35 mm. The elastic modulus of the particular string is not known; therefore, we referred to literature for typical elastic moduli for steel strings of musical instruments⁸ and assumed that $E = 2 \times 10^9$ N/m².

The longitudinal input admittance function has been obtained by exciting the tuning pin with an impulse hammer and measuring its velocity with a laser vibrometer. For accuracy, 200 individual hits were averaged. The measured longitudinal admittance around $2f_0$ is shown in Fig. 9 together with the horizontal admittance function. The admittance values corresponding to the first and second harmonics of the third kantele string are also indicated in the figure.

The string has been displaced with a finger by $a_1 = 2$ mm at its midpoint along the bisection of the transverse unit vectors, and then released. The vibrations of the tuning pin are measured with a laser vibrometer. The first and the second harmonics are extracted from the measured signal

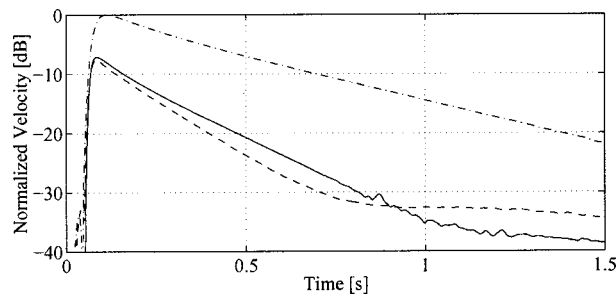


FIG. 10. The extracted velocity magnitude envelopes of the first harmonic (dash-dotted) and the second harmonic (dashed). The calculated second harmonic generated by the T MDF is represented by a solid curve. The measurements were carried out on a modified kantele.

using two fourth-order bandpass Butterworth filters with the center frequencies f_0 and $2f_0$, respectively. The passband of the filters has been set wider than the fundamental frequency descent, and the phase delays introduced by the filters have been compensated. The extracted first and second harmonics are represented in Fig. 10 by dash-dotted and dashed curves, respectively.

The velocity of the second harmonic is calculated as follows. The extracted first harmonic is normalized, downsampled by 2, and scaled by $2a_1^2 \pi^2 (ES/8L^2) = 0.0236$, according to Eq. (7). The oscillatory T MDF term thus calculated is filtered by the measured longitudinal admittance function shown in Fig. 9. The resulting velocity magnitude envelope is represented by a solid curve in Fig. 10.

The calculated and measured velocities are found to be in quantitative agreement up to $t = 0.75$ s. At this instance the magnitude of the second harmonic is approximately 20 dB less than its initial level. From this instance on, another decay rate that is in the vicinity of the transverse second harmonic is observed. The magnitude difference roughly corresponds to the difference between the transmitted and reflected T MDF components, both discussed in the previous subsection. Similar results have been obtained when the recorded tones are analyzed instead of the velocity measurements. In all measurements, the instance at which the transmitted and reflected T MDF components become comparable in magnitude varies between $t = 0.5$ and $t = 1$ s.

The assumption about the rigid terminations dictates that the admittance and consequently the velocity at the tuning pin should vanish. However, as Fig. 9 reveals, the tuning pin in practice has a nonvanishing velocity. In order to resolve this conflict, we may correct the eigenfrequencies and the damping coefficients in Eq. (5) using perturbation calculations.²⁶ However, these perturbations are not crucial for a qualitative description of the nonlinear phenomena of the kantele, as may be justified from Fig. 10.

F. Contribution of the body

The discussion so far explains the generation of the second harmonic in a kantele tone, but it does not account for the high initial magnitude of this component [see Fig. 6(b)]. This difference may be explained by the body responses to tuning peg impulse excitation in three orthogonal directions, as shown in Fig. 11. The measurements were carried out in

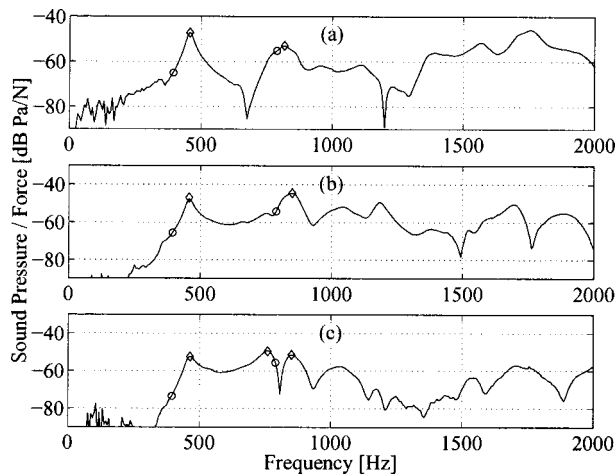


FIG. 11. Sound radiation from the kantele body as a response to (a) vertical; (b) horizontal; and (c) longitudinal driving forces at the third tuning pin. The low-frequency peaks of the radiation functions are indicated by diamonds, whereas the frequencies of the fundamental ($f_0=394.3$ Hz) and second harmonic of the attached string are indicated by circles.

an anechoic chamber. The instrument was held as the player would hold it in a typical performance, i.e., on his/her lap. The tuning pins were struck with an impulse hammer (PCB 086C02), and the response was recorded with a microphone (B&K 4145), fixed at a distance of 1 m. For accuracy, magnitude responses of 200 individual hits were averaged for each direction. Only the low-frequency response is given in the figure. The resonances of the body are represented by diamonds, and the frequencies of the first and second harmonic are indicated with circles.

The lowest resonances occur at 457 Hz for both the vertical and horizontal responses, and at 463 Hz for the longitudinal response. Note that four strings of the kantele are tuned below these frequencies (cf. Table I), unlike the other Baltic psalteries that have typically two or three resonances within the tuning range.⁷ Other resonances can be observed at 817 and 850 Hz for vertical and horizontal directions, respectively. The peak at 850 Hz is also present in the longitudinal response, among a closely spaced peak at 758 Hz. The magnitude levels corresponding to the fundamental frequency ($f_0=394.3$ Hz) are about 20 dB lower compared to the lowest resonance for all responses, indicating that the first harmonic is not efficiently radiated. The second harmonic, on the other hand, is coupled to strong body resonances for each direction, and therefore it is radiated efficiently. Note that the levels corresponding to the second harmonics are comparable in each direction. A strong coupling to a body resonance decreases the decay times of the corresponding harmonics.²⁶ This may explain why the measured second harmonic decays slightly faster than the calculated one in Fig. 10.

For the sake of completeness, we also present a brief summary of the measurements we conducted on the traditional kantele that has a sound hole (see Fig. 1). In a typical playing condition, i.e., when the instrument is played on the lap of the player, the back-plate resonances are partially damped out. At the low-frequency end, the sound hole essentially couples the lowest soundboard resonance and the cav-

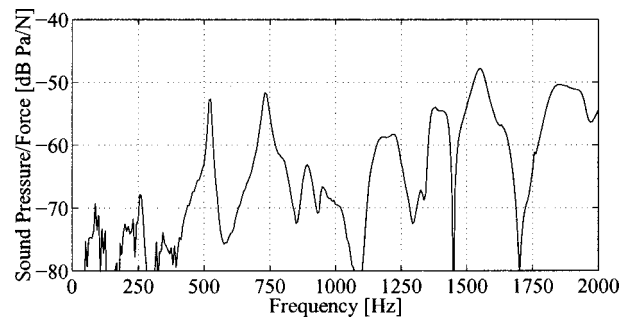


FIG. 12. Sound radiation from the kantele body with a sound hole, as a response to a vertical excitation force at the middle tuning peg.

ity resonance, as in the case of the guitar.²⁷ Figure 12 presents the response of the traditional kantele to the vertical excitation force applied to its third tuning peg in a typical playing condition. The lowest coupled resonance occurs around 522 Hz, where the air flow into the kantele is in the opposite direction of the soundboard vibration. In the second resonance, which is at 732 Hz, the soundboard vibration and the air flow have the same direction.

In every multiple-string instrument, some portion of an individual string's energy is fed to the other strings by various coupling mechanisms. This phenomenon, in which a string vibrates without any direct excitation but is driven only by vibrations of other strings, is called *sympathetic vibration*. Despite the perceptual importance of sympathetic vibrations, there are relatively few analytical treatments of their mechanism,^{26,28} and these treatments usually focus on two strings coupled to the body through a common bridge. However, kantele strings are coupled to the body at one end by individual tuning pins, and at the other by the varras. Altogether, they constitute a system where the resonance characteristics of five strings, five tuning pins, a common body, and a metal bar should be simultaneously taken into account. An analytical treatment of such a system is a challenging task. We chose a simpler approach to examine the total amount of energy transferred from one string to all the others.

We plucked each kantele string in an anechoic room and recorded the total response (with other strings free to vibrate) with a microphone (B&K 4145) fixed at a distance of 1 m. After 2 s, we damped the plucked string with a piece of cotton, and kept on recording the sympathetic vibrations of the other strings. The short-time Fourier transform (STFT) of the analysis data allowed us to specify the damping instance precisely. We calculated rms energy within 500 ms before and after the damping point, averaging 50-ms segments. Repeating this procedure eight times for each string, we obtained the average energy levels just before and after the damping instant. This experiment shows that the energy transfer is most pronounced between the fifth and the first string, followed by the fifth and the third, the fourth and second, and the third and the first strings. Note that all these pairs constitute simple harmonic relationships. These results may be incorporated in the synthesis model, which is the topic of the next section.

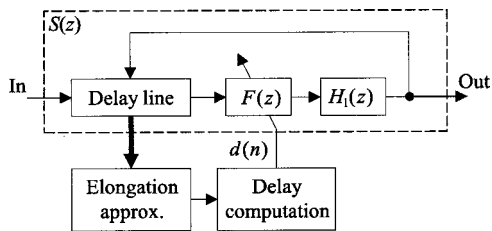


FIG. 13. Computational model $S(z)$ of a vibrating string (the dashed box) where elongation caused by string vibration affects the loop delay through modulation of the delay parameter $d(n)$ of the fractional delay filter $F(z)$. The input signal is an array of sample values that is inserted into the delay line and that corresponds to the initial string slope.

IV. SOUND SYNTHESIS OF THE KANTELE

Even in the earliest studies on nonlinear string vibrations, numerical procedures have been proposed in addition to the more rigorous analytical treatment, since their results are easier to interpret.¹⁴ Model-based sound synthesizers that capture the essentials of the sound production mechanisms of various sound sources are currently being used to test and verify the underlying hypotheses and assumptions.²⁹

In this section, a synthesis model for the kantele is proposed. The suggested model is based on the principles of digital waveguide modeling.³⁰ In an earlier work, kantele tones were synthesized with a linear digital waveguide string model that had an instantaneous nonlinearity at its output.⁶ However, in our current synthesis method,²⁴ the nonlinearity is realized with time-varying signal-dependent elements. The method is based on a recently developed technique to account for the effects of tension modulation caused by variable string displacement.^{13,31} Our aim has been to develop a sound synthesis algorithm that would be sufficiently simple to run in real time, but that would still faithfully reproduce all the peculiar phenomena of the kantele sound described in Sec. III of this paper. In the following, we refer to transverse directions with their explicit names in the formulas to avoid confusion between the vertical spatial variable (see Fig. 4) and the standard DSP unit delay operator z^{-1} .

A. Computational model for a nonlinear string with two polarizations of vibration

Figure 13 shows the block diagram of the nonlinear string model where the tension modulation is incorporated.^{13,31} The digital delay line and the fractional delay filter $F(z)$ together implement the delay that corresponds to the fundamental period of the synthesized sound. Filter $F(z)$ can be implemented using Lagrange interpolation,³² for example. We prefer the FIR Lagrange interpolators to all-pass filters since they have less transient artifacts during parameter updates, despite the losses they introduce at high frequencies.

The filter $H_1(z)$ is called the loop filter, and it is a one-pole filter that implements the frequency-dependent losses of the string^{33,34}

$$H_1(z) = g_1 \frac{1 + a_1}{1 + a_1 z^{-1}}. \quad (8)$$

Tension modulation is realized using a signal-dependent

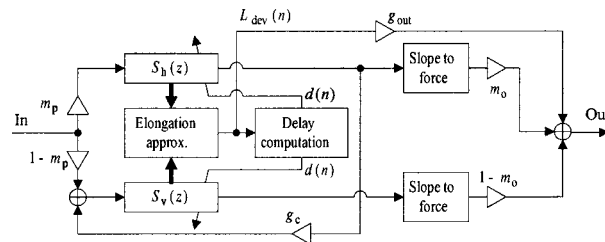


FIG. 14. Dual-mode string model which accounts for the tension modulation. Blocks $S_h(z)$ and $S_v(z)$ are identical with the model shown in Fig. 13.

fractional delay filter. This requires computation of the elongation of the string,^{13,24} which is approximated as a squared sum of the string slope $\partial y/\partial x$. Integration with respect to time converts the instantaneous elongation estimate into deviation of the delay parameter.^{13,31} The model of Fig. 13 can simulate nonlinear transverse string vibration in one polarization of the string (vertical or horizontal).

The model structure for each kantele string consists of two parallel string models, one for each polarization, as depicted in Fig. 14, where $S_h(z)$ and $S_v(z)$ are identical to the model $S(z)$ of Fig. 13.²⁴ As suggested in previous works, the delay line lengths of the two models must be slightly different to generate beats in the synthetic tone.³³⁻³⁵ Notice that the output signal of the horizontal string model leaks to the input of the vertical one (scaled by multiplying coefficient g_c in Fig. 14), as suggested in Ref. 35, so that a revolving polarization is obtained but the system remains stable regardless of the value of the coupling coefficient g_c . While the overall recursive system cannot be guaranteed to remain stable when parameter values of $F(z)$ are time varying, in practice we have not encountered stability problems. It appears that the transient response time of $F(z)$ is faster than the modulation period. Moreover, the losses introduced by $F(z)$ and $H_1(z)$ reduce the Q values of resonances.

The mixing coefficient m_p distributes the initial pluck signal between the horizontal and vertical polarizations, whereas m_o adjusts the contribution of each string to the output signal. Both mixing coefficients have values between 0 and 1.

The total tension of the string, which controls the fractional delay filters in the model of Fig. 14, is approximated by accounting for signals propagating in both waveguide models. In the dual-polarization vibration, the elongation of the string is given by Eq. (2). In the digital waveguide formulation, Eq. (2) is expressed as

$$\begin{aligned} L_{\text{dev}}(n) &= \sum_{k=0}^{\hat{L}_{\text{nom}}-1} \sqrt{1 + s_h^2(n,k) + s_v^2(n,k)} - \hat{L}_{\text{nom}} \\ &\approx \frac{1}{2} \sum_{k=0}^{\hat{L}_{\text{nom}}-1} s_h^2(n,k) + s_v^2(n,k), \end{aligned} \quad (9)$$

where \hat{L}_{nom} is the integer-valued length of the delay line, and $s_h(n,k)$ and $s_v(n,k)$ are the horizontal and vertical slope waves, corresponding to $\partial y/\partial x$ and $\partial z/\partial x$ in Eq. (2), respectively. The instantaneous deviation $L_{\text{dev}}(n)$ needs to be integrated along the string length to obtain the overall deviation, which accounts for the change in wave propagation speed.

The integration is approximated with a digital one-pole filter

$$I(z) = g_p \frac{1 + a_p}{1 + a_p z^{-1}}, \quad (10)$$

where the coefficient values are chosen to be $a_p = 1/\hat{L}_{nom}$ and $g_p = -(1+A)/2$. This choice of coefficient value a_p yields a window length equivalent to that of a running average of \hat{L}_{nom} points, i.e., the nominal length of the delay lines in the string model. Parameter A is the modulation depth related to the string properties and the nominal tension. It can be either calculated from the measured physical quantities of the string, or estimated from the recorded tones, as will be shown below.

The output signal of the one-pole filter is the time-varying delay parameter $d(n)$, which is used to adjust the fractional delay filters in the string models. The direct signal path in Fig. 14 from the elongation estimation block to the output implements the oscillatory term of the TMDF given in Eq. (4) by the selection $g_{out} = T_0 A / L$. For sound synthesis purposes g_{out} may also be used as a parameter to alter the synthetic timbre. Since the synthetic wave variables in the digital waveguides are slope waves, they need to be converted to force waves before the output sum. The force at the tuning pin end may be approximated by¹³

$$f(n, \hat{L}_{nom}) = c_{nom} s(n, \hat{L}_{nom}) \quad (11)$$

for each polarization, where c_{nom} is the nominal transverse wave propagation speed.

B. Parameter estimation and synthesis examples

The nonlinear digital waveguide model of the kantele can produce the features of the instrument only if it is properly calibrated. The parameters of the model may be estimated using formerly proposed techniques for the linear part of the system,³⁴ plus techniques to extract the delay line lengths of the two polarizations and to estimate the appropriate tension modulation parameter A .¹³ The use of the latter two methods is described below.

The calculated or experimentally extracted fundamental frequency difference, discussed in Sec. III B, can be directly converted to the delay line length of $S_h(z)$ and $S_v(z)$. Recall that

$$L_h = \hat{L}_{nom,h} + L_{frac,h} = \frac{f_s}{2f_{0,y}} \quad (12)$$

is the delay length of $S_h(z)$, and a similar expression gives the delay length of $S_v(z)$. The difference of the delay line lengths for both polarizations usually manifests itself in the fractional part, so that the $\hat{L}_{nom,h} = \hat{L}_{nom,v}$ for the first four strings, as can be seen from Table II. The fractional parts are given relative to the sampling interval $T = 1/f_s$. For example $L_{frac,h} = 0.98$ corresponds to $0.98T = 22.22$ microseconds of delay.

There are several ways to obtain the tension modulation parameter A . This parameter can be calculated from the elastic modulus E , the cross-sectional area S , and the nominal tension T_0 of the string if such data are available.¹³ Alternatively, it can be estimated from the fundamental frequency

TABLE II. Integer and fractional parts of the delay line lengths for both polarizations. The sampling frequency is $f_s = 44\,100$ Hz. All quantities are given relative to the sampling interval $T = 1/f_s$.

String	#1	#2	#3	#4	#5
\hat{L}_{nom}	47	53	56	62	69
$L_{frac,v}$	0.27	0.06	0.19	0.03	0.98
$L_{frac,h}$	0.40	0.20	0.35	0.20	1.16

descent of a recorded tone. An example of variation of the fundamental frequency is given in Fig. 15, where the second string has been initially displaced 4.0 mm at its midpoint, and then released. The maximum fundamental frequency here is $f_{0,max} = 424.9$ Hz, and the nominal value is $f_{0,nom} = 409$ Hz. Note that, according to a recent study,³⁶ the overall f_0 variation of 15.9 Hz is well above the perception threshold, and thus clearly audible.

An approximation formula for the A parameter that simulates the observed descent is readily available.¹³ Here, we extract the modulation depth by minimizing the mean-square error between the frequency trajectories of the recorded and synthesized tones. In the synthesis model, the fundamental frequency is $f_{0,nom} = 409$ Hz. The loop filter coefficients [see Eq. (8)] are $g_{1,h} = 0.9946$ and $a_{1,h} = -0.0106$ for the horizontal polarization, and $g_{1,v} = 0.9972$ and $a_{1,v} = -0.0232$ for the vertical polarization. The coupling coefficient is set to a very small value $g_c = 0.0005$, and the input and output mixing parameters are $m_p = 0.55$ and $m_o = 0.44$, respectively. In Fig. 15, the variation of the fundamental frequency of this synthetic tone is presented with a dashed line. The best match in the mean-square sense is obtained with $A = 3876.3$.

The parameter A thus specified, a final example demonstrates that the dual-mode kantele string model can simulate all the essential features of a kantele tone discussed in Sec. III. In this example, the fundamental frequency is set close to that of the third string, i.e., $f_0 = 393.75$ Hz. Note that this value corresponds to an integer delay line length of 56 samples when the sampling frequency is $f_s = 44\,100$ Hz. However, the delay line length difference in both polarizations is preserved in accordance with Table II.

The loop filter coefficients $g_{1,h} = 0.9937$, $g_{1,v} = 0.9983$, $a_{1,h} = -0.0086$, and $a_{1,v} = -0.0232$ provide similar decay times to the extracted decay times of the original kantele tone (see Fig. 10). As in the previous example, $g_c = 0.0005$, $m_p = 0.55$, and $m_o = 0.44$. The TMDF coefficient is deter-

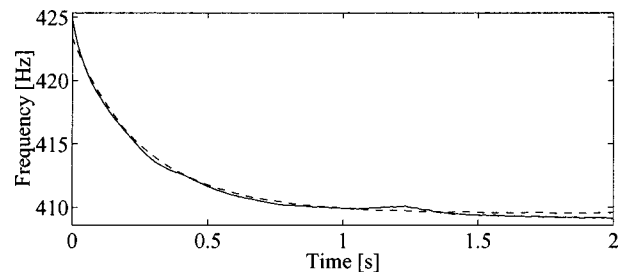


FIG. 15. Variation of the fundamental frequency in a kantele tone (obtained from the modified kantele) resulting from a fortissimo pluck (solid line) and a synthetic tone (dashed line).

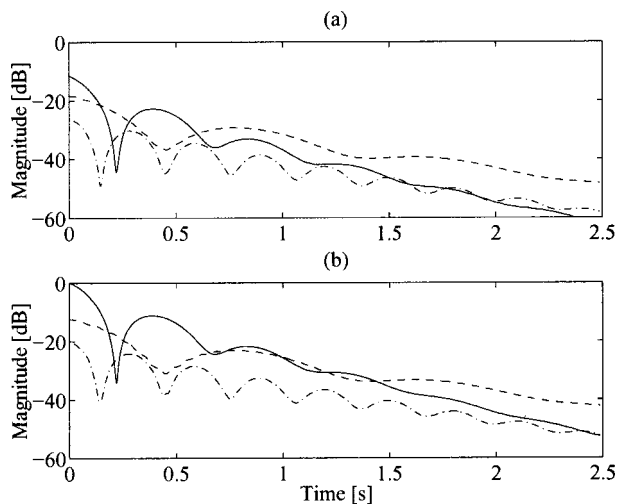


FIG. 16. Envelope trajectories of synthetic kantele tones. The first harmonic is shown with a dashed line, the second one with a solid line, and the third one with a dash-dotted line. (a) A softly plucked tone and (b) a strongly plucked tone. The plucking point is the midpoint of the string. The synthetic tone captures the most important features of a kantele tone as shown in Fig. 5.

mined by using typical values for musical steel strings, and set to $g_{\text{out}} = 823$. A softly plucked and a strongly plucked tone are simulated by setting the initial deflection of the string to 1 and 2 mm, respectively. Figure 16 shows the amplitude envelope trajectories of (a) the softly plucked and (b) the strongly plucked synthetic kantele tones.⁵

A comparison between the synthetic and measured kantele tones (cf. Fig. 5) indicates that the model captures the most important features of a kantele tone, i.e., the beating of the harmonics, and the nonlinear generation and rapid onset of the second harmonic. The differences between the magnitudes of the measured and synthetic harmonics may be explained by noting that the model output shown in Fig. 16 is the composite force at the tuning pin, whereas Fig. 6 represents the radiated sound. It has been shown in Sec. III F that the body causes a filtering effect that inserts an additional 10-dB difference between the first and second harmonic. There are also perceptual differences between the synthetic and measured kantele tones. The parameter estimation method described here is entirely physical. Better results may be obtained if the research results on the perceptual aspects of the pitch glides³⁶ could be included in the parameter estimation procedure.

The simulations can be extended by incorporating a model of the kantele body based on the measurement data presented in Sec. III F. A body filter should be considered, since the *commuted synthesis method*^{37,38} that is based on the linearity and time invariance of the whole system cannot be utilized in the nonlinear kantele model. Various filtering techniques for body modeling are readily available.^{39–42} A body model might improve the perceptual match between the real and synthetic tones. However, the main purpose of the model presented in this paper is to verify and test the causes and effects of the nonlinear phenomena in the kantele tones, and the improvement in the synthesis quality is left for future work.

V. CONCLUSIONS

In this paper the kantele, a traditional Finnish folk music instrument, has been analyzed. The historical and structural properties of the kantele have been briefly overviewed. Two peculiar features of the kantele sound, i.e., the beating of the harmonics and the dominance and generation of the second harmonic, have been described in terms of the physical mechanisms. The cause and effect of the tension modulation driving force (TMDF) have been experimentally demonstrated, and its analytical approximation is presented. Unlike many other stringed instruments, the kantele has been shown to be susceptible to the TMDF.

A more detailed analysis could include various coupling mechanisms between the strings, their terminations (tuning pins and the varras), and the body, and could account for nonlinear coupling of different polarizations or generation of higher harmonics by the transverse components of the forces caused by the tension modulation. However, in this work the unique features of the bridgeless kantele have been found to be related to beating and to the TMDF, and a detailed analysis of other phenomena is left for future research.

The proposed synthesis model, which is based on the principles of digital waveguides and on a nonlinear string model that incorporates tension modulation, has been shown to capture the essential nonlinear properties of the kantele tones. Synthetic sounds produced by the model are in accordance with both the measurements and the analytical approximations. In the present time, the synthesis model includes only the fundamental properties of the real instrument. With increasing computational power, soon it will be feasible to directly incorporate the measured admittance and radiation functions within the sound source models. Then, the correspondence between the real and synthetic instrument could be more striking. Nevertheless, as demonstrated in the paper, even a simple model mimics the essential characteristics of the instrument, and the synthetic sound it produces can be used to verify the underlying assumptions and explanations. The real and synthetic sound examples of the kantele are available via the Worldwide Web.⁵

ACKNOWLEDGMENTS

This research was conducted within the project “Sound Source Models—Analysis, Synthesis, and Coding” financed by the Academy of Finland. The work of C. Erkut has been supported by the Jenny and Antti Wihuri Foundation. The authors would like to thank Dr. Arja Kastinen and Mr. Rauno Nieminen for providing valuable information about the history, form, and function of the instrument.

¹Pronounced 'kän·te·le.

²*The New Grove Dictionary of Musical Instruments*, edited by S. Sadie (MacMillan, London, 1984), pp. 358–359.

³I. Oramo, I. Hämäläinen, K. Virtamo, K. Aho, and M. Elfving, *Suuri musiikkiti-etosanakirja* (Music encyclopedia, in Finnish) (Weilin and Göös, Keuruu, Finland, 1990), pp. 168–171.

⁴*New Larousse Encyclopedia of Mythology*, edited by F. Guirand (Hamlyn, London, U.K., 1986), Chap. 9.

⁵Recorded sound examples are available at: <http://www.acoustics.hut.fi/publications/papers/jasa-kantele/index.html>

⁶M. Karjalainen, J. Backman, and J. Pölkki, “Analysis, modeling, and

- real-time sound synthesis of the kantele, a traditional Finnish string instrument," in Proc. IEEE Int. Conf. Acoust. Speech Signal Processing (Minneapolis, MN, 1993), pp. 229–232.
- ⁷A. Peekna and T. D. Rossing, "The acoustics of baltic psaltery," in Proceedings of the International Symposium on Musical Acoustics (ISMA) (Perugia, Italy, 2001), pp. 437–442.
- ⁸N. H. Fletcher and T. D. Rossing, *The Physics of Musical Instruments* (Springer, New York, 1998), 2nd ed.
- ⁹Special thanks are due to "Ikaalisten soitinrakentajat," who manufactured this special instrument.
- ¹⁰P. Stoica and R. Moses, *Introduction to Spectral Analysis* (Prentice-Hall, Upper Saddle River, NJ, 1997), pp. 146–151.
- ¹¹R. J. Hanson, J. M. Anderson, and H. K. Macomber, "Measurements of nonlinear effects in a driven vibrating wire," J. Acoust. Soc. Am. **96**, 1549–1556 (1994).
- ¹²K. A. Legge and N. H. Fletcher, "Nonlinear generation of missing modes on a vibrating string," J. Acoust. Soc. Am. **76**, 5–12 (1984).
- ¹³T. Tolonen, V. Välimäki, and M. Karjalainen, "Modeling of tension modulation nonlinearity in plucked strings," IEEE Trans. Speech Audio Process. **8**, 300–310 (2000).
- ¹⁴G. F. Carrier, "On the non-linear vibration problem of the elastic string," Q. Appl. Math. **3**, 157–165 (1945).
- ¹⁵C. Valette, "The mechanics of vibrating strings," in *Mechanics of Musical Instruments*, edited by A. Hirschberg, J. Kergomard, and G. Weinreich (Springer, New York, 1995), pp. 116–183.
- ¹⁶G. V. Anand, "Large-amplitude damped free vibration of a stretched string," J. Acoust. Soc. Am. **45**, 1089–1096 (1969).
- ¹⁷J. W. Miles, "Resonant, nonplanar motion of a stretched string," J. Acoust. Soc. Am. **75**, 1505–1510 (1984).
- ¹⁸C. E. Gough, "The nonlinear free vibration of a damped elastic string," J. Acoust. Soc. Am. **75**, 1770–1776 (1984).
- ¹⁹Z. C. Feng, "Does nonlinear intermodal coupling occur in a vibrating stretched string?," J. Sound Vib. **182**, 809–812 (1995).
- ²⁰N. Tuffillaro, "Nonlinear and chaotic string vibrations," Am. J. Phys. **30**, 408–414 (1989).
- ²¹B. E. Richardson, "String instruments: Plucked," in *Encyclopedia of Acoustics*, edited by M. J. Crocker (Wiley, New York, 1997), Vol. 4, pp. 1627–1634.
- ²²T. Tolonen, C. Erkut, V. Välimäki, and M. Karjalainen, "Simulation of plucked strings exhibiting tension modulation driving force," in Proc. Int. Comput. Music Conf. (Beijing, China, 1999), pp. 5–8.
- ²³H. A. Conklin, "Generation of partials due to nonlinear mixing in a stringed instrument," J. Acoust. Soc. Am. **105**, 536–545 (1999).
- ²⁴V. Välimäki, M. Karjalainen, T. Tolonen, and C. Erkut, "Nonlinear modeling and synthesis of the kantele—A traditional Finnish string instrument," in Proc. Int. Comput. Music Conf. (Beijing, China, 1999), pp. 220–223.
- ²⁵X. Boutillon and G. Weinreich, "Three-dimensional mechanical admittance: Theory and new measurement method applied to the violin bridge," J. Acoust. Soc. Am. **105**, 3524–3533 (1999).
- ²⁶C. E. Gough, "The theory of string resonances on musical instruments," Acustica **49**, 124–141 (1981).
- ²⁷O. Christensen and B. B. Vistisen, "Simple model for low-frequency guitar function," J. Acoust. Soc. Am. **68**, 758–766 (1980).
- ²⁸G. Weinreich, "Coupled piano strings," J. Acoust. Soc. Am. **62**, 1474–1484 (1977).
- ²⁹G. Essl and P. R. Cook, "Measurements and efficient simulations of bowed bars," J. Acoust. Soc. Am. **108**, 379–388 (2000).
- ³⁰J. O. Smith, "Physical modeling using digital waveguides," Comput. Music J. **16**, 74–91 (1992).
- ³¹V. Välimäki, T. Tolonen, and M. Karjalainen, "Plucked-string synthesis algorithms with tension modulation nonlinearity," in Proc. IEEE Int. Conf. Acoust. Speech Signal Processing (Phoenix, AZ, 1999), pp. 977–980.
- ³²T. Laakso, V. Välimäki, M. Karjalainen, and U. K. Laine, "Splitting the unit delay-tools for fractional delay filter design," IEEE Signal Process. Mag. **13**, 30–60 (1996).
- ³³D. A. Jaffe and J. O. Smith, "Extensions of the Karplus–Strong plucked-string algorithm," Comput. Music J. **7**, 56–69 (1983).
- ³⁴V. Välimäki, J. Huopaniemi, M. Karjalainen, and Z. Jánosy, "Physical modeling of plucked string instruments with application to real-time sound synthesis," J. Audio Eng. Soc. **44**, 331–353 (1996).
- ³⁵M. Karjalainen, V. Välimäki, and T. Tolonen, "Plucked-string models: From the Karplus–Strong algorithm to digital waveguides and beyond," Comput. Music J. **22**, 17–32 (1998).
- ³⁶H. Järveläinen and V. Välimäki, "Audibility of initial pitch glides in string instrument sounds," in Proc. Int. Comput. Music Conf. (Havana, Cuba, 2001).
- ³⁷J. O. Smith, "Efficient synthesis of stringed musical instruments," in Proc. Int. Comput. Music Conf. (Tokyo, Japan, 1993), pp. 64–71.
- ³⁸M. Karjalainen, V. Välimäki, and Z. Jánosy, "Towards high-quality sound synthesis of the guitar and string instruments," in Proc. Int. Comput. Music Conf. (Tokyo, Japan, 1993), pp. 56–63.
- ³⁹K. Bradley, M. H. Cheng, and V. L. Stonick, "Automated analysis and computationally efficient synthesis of acoustic guitar strings and body," in Proc. IEEE Workshop of Applications of Signal Processing to Audio and Acoustics (New Paltz, NY, 1995), pp. 238–241.
- ⁴⁰M. Karjalainen and J. O. Smith, "Body modeling techniques for string instrument synthesis," in Proc. Int. Comput. Music Conf. (Hong Kong, 1996), pp. 232–239.
- ⁴¹P. R. Cook and D. Trueman, "NBody: Interactive multidirectional musical instrument body radiation simulators, and a database of measured impulse responses," in Proc. Int. Comput. Music Conf. (Ann Arbor, MI, 1998), pp. 353–356.
- ⁴²M. Karjalainen, V. Välimäki, H. Penttinen, and H. Saastamoinen, "DSP equalization of electret film pickup for the acoustic guitar," J. Audio Eng. Soc. **48**, 1183–1193 (2000).